


# Validation of Raman spectroscopy as a tool for mapping transport parameters in inhomogeneous N-doped 4H-SiC

Hannes Hergert<sup>1</sup>  | Matthias T. Elm<sup>1,2,3</sup>  | Peter J. Klar<sup>1,2</sup>

<sup>1</sup>Zentrum für Materialforschung (ZfM/LaMa), Justus-Liebig-Universität, Giessen, Germany

<sup>2</sup>I. Physikalisches Institut, Justus-Liebig-Universität, Giessen, Germany

<sup>3</sup>Physikalisch-Chemisches Institut, Justus-Liebig-Universität, Giessen, Germany

## Correspondence

Hannes Hergert, Zentrum für Materialforschung (ZfM/LaMa), Justus-Liebig-Universität, Giessen, Germany.  
Email: [hannes.hergert@physik.uni-giessen.de](mailto:hannes.hergert@physik.uni-giessen.de)

## Funding information

Deutsche Forschungsgemeinschaft, Grant/Award Number: 498993886; Hessisches Ministerium für Wissenschaft und Kunst, Grant/Award Number: ERDF-Innovation Laboratory; European Union; Heisenberg Program, Grant/Award Number: EL863/6-1

## Abstract

We assess Raman spectroscopy as a tool for fast and non-invasive mapping of charge carrier density and carrier mobility in inhomogeneously doped 4H-SiC. For this purpose, we compare values of these transport parameters obtained by magneto-transport and Raman measurements of N-doped 4H-SiC. The comparison is not straightforward. The effective charge density and mobility, which are obtained from resistivity and Hall measurements by employing the commonly used effective one-band model, deviate from the values extracted by applying the established line-shape models for describing the longitudinal optical phonon coupled (LOPC) modes in the Raman spectra. Differentiating between free and localized carriers in the framework of a three-band transport model confirms that only the free charge carriers in the conduction band of N-doped 4H-SiC contribute to the LOPC Raman signal and their density agrees well with that obtained by the line shape analysis. The agreement of the mobility values is good keeping in mind that different frequencies of the applied electric fields are used in the two approaches, i.e., dc-transport measurements at 0 Hz and ac-fields of the exciting laser at about 500 THz. Moreover, the excitation of electrons into the conduction band by the laser, which is inherent to the Raman experiment, causes differences in the temperature dependence of the carrier density compared with the electrical transport data.

## KEYWORDS

4H-SiC, carrier concentration, electrical transport, line shape analysis, LOPC (longitudinal optical Plasmon coupled) mode

## 1 | INTRODUCTION

Siliciumcarbid (SiC) has gained much interest in recent years in the context of high-power applications, e.g., in electric vehicles. SiC is suitable for electronic and optoelectronic components that operate under demanding conditions, due to its outstanding thermal and electrical

properties. In particular, its wide band gap makes SiC applicable for high power and high-temperature devices.<sup>1,2</sup> Crystalline SiC may occur in various polytypes, however, of those only the 4H and 6H polytypes are available as large single crystals. Corresponding SiC wafers are the basis of devices in the various fields of application.<sup>3–5</sup> A fast screening of such wafers prior to

This is an open access article under the terms of the [Creative Commons Attribution-NonCommercial-NoDerivs](https://creativecommons.org/licenses/by-nc-nd/4.0/) License, which permits use and distribution in any medium, provided the original work is properly cited, the use is non-commercial and no modifications or adaptations are made.

© 2023 The Authors. *Journal of Raman Spectroscopy* published by John Wiley & Sons Ltd.

electronic device fabrication, e.g., for identifying structural and doping inhomogeneity, is highly desirable for high-yield device production.<sup>6</sup>

Magneto-transport measurements are the established method for in-depth studies of electric transport phenomena in semiconductors.<sup>7,8</sup> Amongst others, measurements of the specific resistivity and the Hall coefficient in low fields yield charge carrier density and mobility when analysed with appropriate microscopic models. Furthermore, temperature-dependent data help to differentiate between localized and extended band states of electrons or holes involved in the transport. They also give insight into the dominant transport mechanisms such as hopping, diffusive or ballistic transport as well as into the underlying microscopic scattering mechanisms in case of diffusive transport. The approach is very powerful and reliable for determining transport parameters of semiconductor bulk material, nanostructures and devices.<sup>9–11</sup> Corresponding in-depth studies contribute significantly to a better understanding of electronic transport in solids and, in particular, semiconductors. A major disadvantage is, however, that electric transport measurements in general need a time-consuming sample preparation prior to the actual measurement process. Reliable electrical transport measurements for obtaining charge-carrier density and mobility of the wafer material require defined electrical contact geometries, ohmic behaviour of the contacts, and the application of external magnetic fields. Consequently, this approach is invasive and rather slow, thus, not suitable for in-line characterization of entire wafers in wafer production or device fabrication processes.

Optical spectroscopic inspection is widely employed in wafer screening as no dedicated sample preparation is required and a fast spatial mapping of the wafer is possible. A suitable optical spectroscopic method for screening N-doped SiC wafers in terms of carrier density and mobility may be offered by Raman spectroscopy.<sup>12,13</sup> Raman spectra of the longitudinal-optical (LO) phonon region in polar semiconductors like SiC can yield information about charge carrier density and mobility of doped samples. The underlying physical effect is that the LO phonon couples to the free charge carriers introduced by doping giving rise to longitudinal optical phonon coupled (LOPC) modes. The appearance of the LOPC mode in Raman spectra depends strongly on the charge carrier density and carrier mobility. Appropriate line shape analysis of the phonon-like LOPC mode in the Raman spectra yields charge carrier density and carrier mobility values in the case of a doped semiconductor. Corresponding theoretical models are well established.<sup>8,14</sup> In addition when employing Raman microscopy, the transport properties can be determined locally with a spatial resolution down to the  $\mu\text{m}$ -scale. In contrast, electrical transport

measurements typically average the properties on a considerably larger scale. If appropriately validated, Raman spectroscopy of the LOPC mode may turn out to be a viable alternative to magneto-transport measurements for determining carrier densities and mobilities. This holds, in particular, for studying samples with large doping inhomogeneity or for application in fast wafer screening.

There are several reports available in the literature dealing with the analysis of the LOPC mode of SiC in terms electronic transport properties.<sup>8,14–16</sup> However, the corresponding comparison of charge carrier density and mobility values extracted from the Raman and the electric transport measurements on the same SiC samples is restricted to room temperature conditions only. Here, we perform a detailed comparison of temperature-dependent Raman and electrical transport results. By a careful analysis, we reveal the range of application of Raman measurements as a tool for determining electrical transport properties of N-doped SiC as well as its limitations for doping concentrations of some  $10^{18} \text{ cm}^{-3}$ .

## 2 | EXPERIMENTAL DETAILS

We investigate different samples from a highly N-doped 4H-SiC wafer with orientation of the surface normal 4 degrees off the hexagonal c-axis (see also Figure S1a)). The wafer diameter is 100 mm and the wafer thickness 350  $\mu\text{m}$ . The wafer is of engineering-grade quality and was bought from SiCrystal GmbH. The wafer was cut into 69 equally sized, square-shaped chips (1  $\text{cm}^2$ ). All chips were studied by optical inspection and Raman spectroscopy. Four of those were carefully selected for further examination, i.e., for a thorough comparison of temperature-dependent Raman and magneto-transport measurements. The selection was based on the colour impression of these chips, two were selected from the brighter area of the wafer and two from the darker spot. The labelling of the samples corresponds to the position on the wafer (see Figure S1). Four Mo contacts were evaporated onto the corners of each of the selected SiC chips. For this purpose, the chips were ultrasonically cleaned with acetone and methanol, dried in a nitrogen flux, masked and subsequently mounted in an RF magnetron sputtering chamber operating with an Ar plasma and a Mo metallic target. After pumping down to a base pressure of  $2.8 \times 10^{-4} \text{ Pa}$ , the growth of the Mo thin contact pads was initiated. The contacts were annealed at 1000°C for 60 seconds after growth in order to diffuse Mo into the SiC below the contact pads. Applying copper wires with conductive silver paste to the four Mo pads yielded ohmic contacts required for the magneto-transport measurements in van-der-Pauw geometry.

The transport measurements were performed in an Oxford Instruments superconducting magnet system with a variable temperature insert enabling temperature-dependent measurements between 1.5 and 300 K in magnetic fields up to 10 T. The magneto-resistivity and Hall measurements were performed in Van-der-Pauw geometry.

Raman measurements were conducted in backscattering geometry using a Renishaw InVia Raman microscope system equipped with a charge-coupled device camera. A He-Ne laser with an excitation wavelength of 633 nm, a focal spot diameter of 1  $\mu\text{m}$ , and a laser power of 7 mW was employed in all experiments. Raman spectra were recorded in the relative wavenumber range from 200 to 1200  $\text{cm}^{-1}$  with a spectral resolution of 1.5  $\text{cm}^{-1}$ . Temperature-dependent measurements were performed in the temperature range between 80 and 700 K using a Linkam Stage THMS600, which can be cooled by liquid nitrogen or heated. All measurements were calibrated and performed with an integration time of 10 s.

### 3 | RESULTS AND DISCUSSION

Figure 1 depicts the transport parameters extracted from the temperature-dependent resistivity and Hall measurements in the temperature range between 1.5 and 300 K. Exemplarily, the plots of the resistivity curves of two chips, No 15 and No 44, of the same N-doped SiC wafer are depicted in Arrhenius representation in Figure 1A. The measured resistivity of both chips decreases with increasing temperature. However, the value at room temperature of the resistivity of chip No. 44 is about five times lower than that of No 15 reflecting the inhomogeneity of the N doping of the wafers. Furthermore, the resistivity curves in the Arrhenius plots strongly deviate

from a linear behaviour indicating that the dominant carrier excitation process or transport process changes as a function of temperature.

Analysing the Hall and resistivity data, i.e., electrical resistivity  $\rho$  and Hall constant  $R_H$ , within a one-band Drude model in the low field limit yields the effective carrier concentration  $n_{\text{eff}}$  and an effective mobility  $\mu_{\text{eff}}$  at each temperature:

$$n_{\text{eff}}(T) = \frac{1}{qR_H(T)}, \quad (1)$$

$$\mu_{\text{eff}}(T) = \left| \frac{R_H(T)}{\rho(T)} \right| \quad (2)$$

where  $q$  is the charge of the carrier, i.e.  $q = -e$  for electrons. Plots of the effective carrier concentration and the effective mobility vs inverse temperature are shown in Figure 1B,C, respectively. The effective carrier concentration  $n_{\text{eff}}$  is almost constant for both specimens below 5 K and then rises exhibiting maxima at 12 K and at 34 K for No 15 and No 44, respectively, prior to decreasing again and reaching a minimum at 117 and 174 K. Finally, the carrier concentration increases again when the measurement temperature approaches room temperature from below. This is not what is expected in case of a moderately n-doped semiconductor described by a parabolic conduction band (CB) with its band edge at  $E_{\text{CB}}$  and shallow donors at a discrete donor level located at  $E_{\text{D}}$  below CB. Starting from 0 K, one would anticipate first an exponential rise of the carrier concentration with increasing temperature, then a saturation region followed by another stronger exponential rise at very high temperatures. The characteristic temperature regions are the freeze-out region at low temperatures, where carriers are

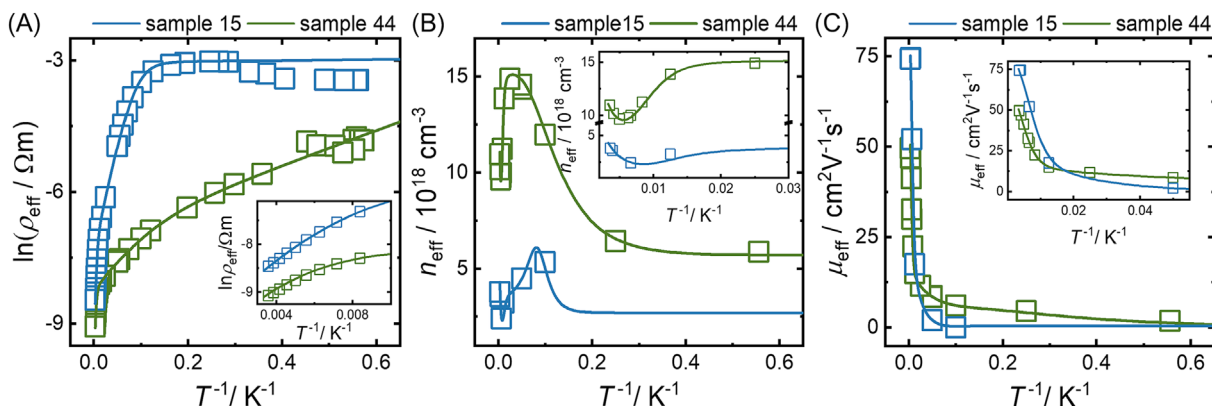
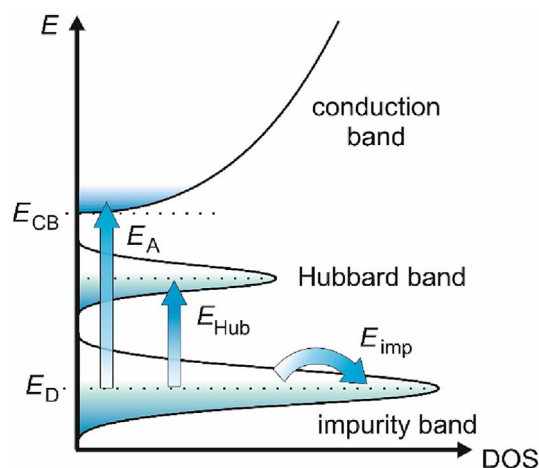


FIGURE 1 Temperature-dependent transport properties of the SiC chips no 15 (blue) and no 44 (green) with insets for the high-temperature region: (A) resistivity, (B) effective carrier density, and (C) effective electron mobility. The solid lines represent curves obtained by fitting a three-band model to the measurement results (squares).

excited from the donors to the CB and the carrier concentration increases exponentially with an activation energy  $E_A = E_{CB} - E_D$ , followed by the saturation range in the intermediate temperature range, where all donor electrons are excited into the CB and the carrier concentration is almost constant. Finally, at higher temperatures, the intrinsic region gives rise to another exponential increase of  $n_{\text{eff}}$ . In the intrinsic region, all donor electrons are in the CB, but additional thermal excitation across the band gap starts to play a role. Thermally activated electrons and holes act as additional free carriers in the CB and valence band (VB). The transition temperatures between the regimes depend on the band structure. As a rule of thumb, the transition from freeze-out region to saturation region occurs at  $E_A/(k_B T) \cong 1$ , while the transition between saturation region and intrinsic region occurs where  $E_{CB}/(2k_B T) \cong 1$  assuming here that the valence band edge is located at  $E_{VB} = 0$ . The isolated nitrogen donor has a depth between 50 and 100 meV depending on the local site.<sup>17–20</sup> Thus, the onset of the saturation is about expected at about 600 K. The onset temperature of the intrinsic region in SiC is way above the highest temperature of 700 K where we performed experiments due to a band gap energy  $E_{CB} - E_{VB} = 3$  eV for 4H-SiC in the temperature range studied.<sup>21</sup> Thus, only the free carriers in the CB contribute to the electric transport up to 300 K, i.e., the temperature range covers almost solely the freeze-out region, which is the justification for using a one-band Drude model in such a scenario.

However, the observed temperature dependence of the resistivity of the two specimens in the range from 1.5 to 300 K is not compatible with the scenario described above, as the slope of the Arrhenius plot changes about three times in the temperature range studied. Furthermore, the effective carrier concentration in Figure 1B is not compatible with a one-band description as it decreases with increasing temperature in the intermediate temperature region. Moreover, the effective mobility takes on very low values below 20 K, which are indicative for hopping transport and not compatible with solely free carrier transport in the CB. These findings together with effective carrier concentrations in the range of  $10^{18}$  to  $10^{19}$  cm<sup>-3</sup> for both specimens suggest that we are dealing with a highly doped semiconductor material, where the electronic states are close to the Mott or insulator-to-metal transition and a one-band description fails.

In such highly doped semiconductors, parallel transport paths involving different electronic states or bands and possibly different transport processes contribute simultaneously to the electronic transport in the temperature range considered.<sup>22,23</sup> Typically, a particular transport path dominates the resistivity in a specific



**FIGURE 2** Schematic diagram of the density of states for the investigated N-doped 4H-SiC samples illustrating the applied three-band model.  $E_A$  and  $E_{\text{Hub}}$  represent the excitation of electrons into the conduction or the Hubbard band, respectively.  $E_{\text{imp}}$  indicates electron hopping within the impurity band.

temperature region. This can be understood based on the scheme shown in Figure 2. It sketches the density of states arising from the intrinsic conduction band states and the donor states for the situation corresponding to a highly doped semiconductor below the Mott transition. The CB density of states is still almost unaffected, but the donor states start to form a broad impurity band due to the overlapping donor electron wave functions. Its width increases with increasing donor concentration until it merges with the conduction band at a critical carrier concentration  $n_c$  corresponding to the Mott transition. For carrier concentrations below  $n_c$ , carriers are still thermally excited from the impurity band into the conduction band changing their character from localized to free carriers (process 1). Thus, the activation energy  $E_A$  is non-zero, but is reduced compared to the low or moderate doping case. This transport process dominates at higher temperatures. However, transport may also take place within the impurity band. Electrons bound to donors may hop from a neutral donor state  $D^0$  to an ionized donor state  $D^+$  (process 3). Such  $D^+$  states may be present even at the lowest temperatures, if the n-type semiconductor is partially compensated, i.e., a residual amount of acceptors is also present in addition to the intentionally introduced donor doping. A certain degree of compensation usually occurs in real samples. Such hopping transport within the impurity band is dominant at low temperatures and is typically characterized by a very low activation energy  $E_{\text{imp}}$  and very low mobilities. In the intermediate temperature range, another process may occur and become dominant. It is represented by the

so-called Hubbard band located between the impurity and the CB band. This representation is somewhat misleading as the Hubbard band represents a process, which cannot be described within a one-electron band structure. It corresponds to the hopping of a donor electron from a  $D^0$  to another  $D^0$  turning the latter into a  $D^-$  (process 2). Because of the Coulomb interaction between the two outer electrons of the  $D^-$  final state (Coulomb penalty) the activation energy  $E_{\text{Hub}}$  of this hopping process between neutral  $D^0$  is considerably larger than that between  $D^0$  and  $D^+$ , but  $E_{\text{Hub}}$  is smaller than  $E_A$ . As rule of thumb, it holds  $E_{\text{Hub}} \cong 0.1 E_A$ . The contributions of the three transport processes add up to the total conductivity of the specimen:

$$\sigma_{\text{tot}}(T) = \sigma_1(T) + \sigma_2(T) + \sigma_3(T) \quad (3)$$

Typically process 1 is described as diffusive transport (i.e., thermally activated carrier density in the CB with a, for simplicity, temperature-independent mobility  $\mu_{\text{CB}}$ ), whereas processes 2 and 3 are described by hopping (i.e., the mobilities are thermally activated, whilst the corresponding carrier densities  $n_{\text{hop}}$  and  $n_{\text{Hub}}$  are assumed to be constant).<sup>23</sup> In zero magnetic field, it holds:

$$\sigma_1(T) = en_{\text{CB}}(T)\mu_{\text{CB}} = e\mu_{\text{CB}}n_{\infty,\text{CB}} \exp\left(-\frac{E_A}{k_B T}\right) \quad (4)$$

$$\sigma_2(T) = en_{\text{Hub}}\mu_{\text{Hub}}(T) = en_{\text{Hub}}\mu_{\infty,\text{Hub}} \exp\left(-\frac{E_{\text{Hub}}}{k_B T}\right) \quad (5)$$

$$\sigma_3(T) = en_{\text{imp}}\mu_{\text{imp}}(T) = en_{\text{imp}}\mu_{\infty,\text{imp}} \exp\left(-\frac{E_{\text{imp}}}{k_B T}\right) \quad (6)$$

where  $T$  denotes the absolute temperature and  $k_B$  is the Boltzmann constant. The quantity  $n_{\infty,\text{CB}}$  describes the saturation value of  $n_{\text{CB}}$  for infinite temperature in this parameterization, and similarly  $\mu_{\infty,\text{imp}}$  and  $\mu_{\infty,\text{Hub}}$  are the saturation values of the hopping mobilities at infinite temperature. For simplicity, we assume that the average motion of the electrons is determined by the generalized Lorentz force as well as the underlying scattering processes. In addition, we assume that the transport in the hexagonal c-plane is isotropic (which is still a good approximation for the 4H-SiC wafer used despite its  $4^\circ$  off-axis surface orientation) and that the Hall scattering factor is 1.<sup>24–26</sup> Based on these assumptions, an external magnetic field applied perpendicular to the sample plane yields additional off-diagonal tensor elements of the conductivity tensor. These off-diagonal elements cause the

Hall current in the sample plane at non-zero field. The resistivity tensor in the presence of a magnetic field is obtained by inverting the total conductivity (given by the sum of the conductivity tensors of the three transport processes) in the presence of the magnetic field.<sup>23</sup> By expanding the resistivity tensor elements with respect to the magnetic field in a Taylor series about zero-field, one obtains for the effective resistivity in zero-field and the Hall coefficient the following expressions:

$$\rho_{\text{eff}}(T) = \frac{1}{e(\sum_{i=1}^3 n_i(T)\mu_i(T))} \quad (7)$$

$$R_{\text{H}}(T) = \frac{1}{-en_{\text{eff}}(T)} = \frac{\sum_{i=1}^3 n_i(T)\mu_i^2(T)}{-e\sum_{i=1}^3 n_i^2(T)\mu_i^2(T)} \quad (8)$$

Inserting Equations (7) and (8) into Equation (1) yields the effective carrier concentration  $n_{\text{eff}}(T)$  and the effective mobility  $\mu_{\text{eff}}(T)$  as a function of temperature in dependence on the transport parameters of the three-band model. Also shown in Figure 1 is a comparison of the experimental values for the temperature dependence of the effective resistivity  $\rho_{\text{eff}}(T)$  and of the two extracted quantities  $n_{\text{eff}}(T)$  and  $\mu_{\text{eff}}(T)$  with corresponding curves obtained by the three-band model where the model parameters were adjusted to yield the best agreement. For both specimens studied, the three-band model can reproduce the rather complex temperature dependence of all three quantities. In particular, the fitted curve of the effective resistivity exhibits the changes of slope occurring in the temperature range studied. An alteration of the slope in the Arrhenius representation used is associated with a change of the effective activation energy. It reflects that the three transport processes introduced in the model dominate in different temperature regions, as anticipated from the discussion above. Furthermore, the model can reproduce maximum and minimum in the Arrhenius representation of the effective carrier density at high temperatures for both specimens. The extrema arise as the effective carrier concentration is determined by the sum of the carriers in each band weighted by their mobilities (c.f. Equation (8)). At low temperatures,  $n_{\text{eff}}$  is given by the electrons in the impurity band, which exhibit a low mobility value. With increasing temperature, electrons are thermally excited into the Hubbard band with higher mobility and, thus,  $n_{\text{eff}}$  increases. In the intermediate temperature range, electrons are also excited into the conduction band. Although their concentration is still lower than that in the Hubbard band, they determine  $n_{\text{eff}}$  due to their high mobility in the CB resulting in a decrease of  $n_{\text{eff}}$ . The effective carrier concentration increases again as the effective carrier concentration

at higher temperatures is determined by the concentration of electrons, which are thermally excited into the conduction band. With regard to effective mobility, the model can grab the temperature-induced transition from dominant hopping transport with very low effective mobilities at low temperatures to diffusive CB band transport with much higher mobilities at higher temperatures. The model parameters of the best fit are summarized in the supporting information (see Table S1) for all four chips investigated. The average activation energy  $E_A$  of the nitrogen impurity band for all chips studied of about 40 meV is somewhat lower than the range of values of the donor binding energy given for an isolated donor in the literature of 50 to 100 meV.<sup>17–20</sup> The reason is that the broadening of the impurity band due to the interacting donor wave functions causes an effective reduction of the donor binding energy which is proportional to the donor density to the power 1/3.<sup>9,27–29</sup>

Raman spectroscopy can explore the coupling between phonons and free electrons to extract electronic transport parameters. In the case of semiconductors with at least partially polar bonding, LO phonons induce a Coulomb potential which couples via Froehlich interaction with the electron plasma<sup>30</sup> and forms the LOPC mode. In the Drude framework, the characteristic properties of the electron plasma are given by the plasma frequency  $\omega_p$  and the plasmon-damping constant  $\gamma_p$ :

$$\omega_p^2 = \frac{4\pi n_{\text{eff,R}} e^2}{\epsilon_0 \epsilon_\infty m^*} \quad (9)$$

$$\gamma_p = \frac{e}{m^* \mu_{\text{eff,R}}} \quad (10)$$

where  $\epsilon_\infty$  and  $\epsilon_0$  are the high-frequency dielectric constant and the vacuum permittivity,  $m^*$  is the effective electron mass,  $n_{\text{eff,R}}$  and  $\mu_{\text{eff,R}}$  are the effective charge carrier density and the effective electron mobility. The subscript index R denotes for clarity that the values are obtained by analysing the Raman data.

The LOPC mode as a coupled mode differs from the pure LO phonon mode in terms of Raman shift and line shape. Its appearance depends on the properties of the free-electron plasma given in the applied electric field. In the Raman experiment, the applied electric field is not a dc field as in the magneto-transport experiments, but the electric part of the electromagnetic light wave of the laser used as excitation source. Detailed derivations of the line shape model can be found in.<sup>8,15,31,32</sup> The intensity profile of the LOPC Raman signal can be described by:

$$I_{\text{LOPC}}(\omega) = k \cdot A(\omega) \cdot \text{Im} \left( \frac{-1}{\epsilon(\omega)} \right) + Y \quad (11)$$

where  $k$  is a constant scaling factor and  $Y$  represents a constant offset accounting for a possible background. The total dielectric function  $\epsilon(\omega)$  and  $A(\omega)$  are given by:

$$\epsilon(\omega) = \epsilon_\infty \left( 1 + \frac{\omega_{\text{LO}}^2 - \omega_{\text{TO}}^2}{\omega_{\text{TO}}^2 - \omega^2 - i\omega\Gamma} - \frac{\omega_p^2}{\omega(\omega + i\gamma_p)} \right) \quad (12)$$

$$A(\omega) = 1 + \left( \frac{2 \cdot C \cdot \omega_T^2}{\Delta(\omega)} \right) \left( \omega_p^2 \gamma_p (\omega_{\text{TO}}^2 - \omega^2) - \omega^2 \Gamma (\omega^2 + \gamma_p^2 - \omega_p^2) \right) \\ + \left( \frac{C^2 \cdot \omega_T^4}{\Delta(\omega) \cdot (\omega_{\text{LO}}^2 - \omega_{\text{TO}}^2)} \right) \left( \omega_p^2 (\gamma_p (\omega_{\text{LO}}^2 - \omega_{\text{TO}}^2) + \Gamma (\omega_p^2 - 2\omega^2)) \right) \\ + \omega^2 \Gamma (\omega^2 + \gamma_p^2) \quad (13)$$

with

$$\Delta(\omega) = \omega_p^2 \gamma_p \left( (\omega_{\text{TO}}^2 - \omega^2)^2 + \omega^2 \Gamma^2 \right) \\ + \omega^2 \Gamma (\omega_{\text{LO}}^2 - \omega_{\text{TO}}^2) (\omega^2 + \gamma_p^2) \quad (14)$$

where  $\omega_{\text{LO}}$  and  $\omega_{\text{TO}}$  are the LO and TO frequencies of the corresponding undoped material,  $\Gamma$  is the phonon damping constant, and  $C$  the Faust-Henry coefficient.<sup>33</sup> With these expressions, one can correlate the position and the line shape of the LOPC mode with the mobility and the charge carrier density. At low charge carrier densities, the peak position of the LOPC mode solely depends on the effective charge carrier density  $n_{\text{eff,R}}$ , it moves to higher Raman shifts as the charge carrier density increases. At higher charge carrier densities, the Raman shift of the LOPC peak is influenced by both effective mobility  $\mu_{\text{eff,R}}$  and  $n_{\text{eff,R}}$ . Furthermore, the effective mobility  $\mu_{\text{eff,R}}$  affects the line width of the LOPC mode.

Thus, Raman data should also yield values of the effective carrier density and mobility. However, it needs to be validated whether these values agree with those extracted from the magneto-transport data. This is not a priori clear because the applied electric fields, which cause the transport in both cases, differ considerably in terms of frequency. Furthermore, the three-band model accounts for localized and extended electronic states in the description of effective charge density whereas the line shape of the LOPC mode from which the effective carrier density is derived depends on free carrier plasma only. Thus, it needs to be clarified whether the values of effective carrier density extracted at a certain temperature

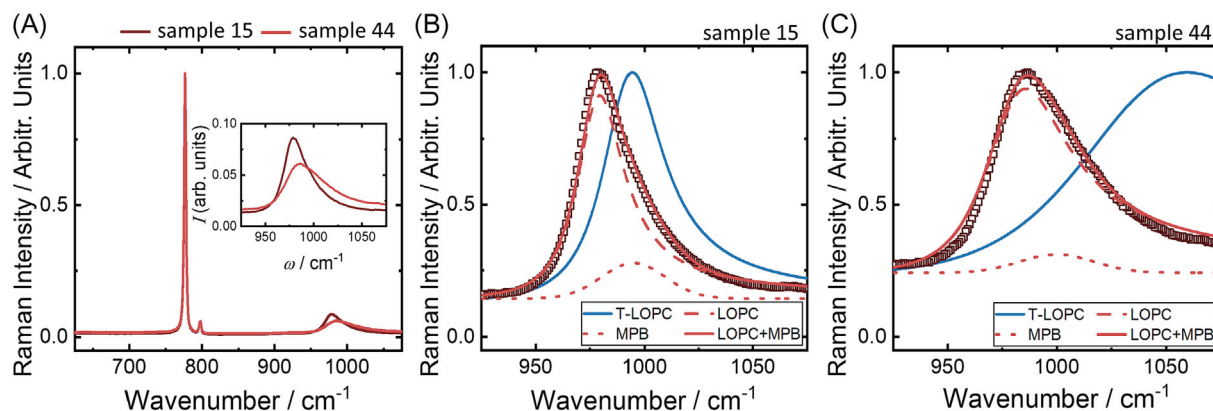


**FIGURE 3** (A) Experimental Raman spectra for chips 15 (dark red) and 44 (bright red) with a closer look onto the LOPC mode in the inset. (B,C) Spectral region of the LOPC mode (squares) for chip 15 and chip 44, respectively. The blue line represents the model for the LOPC mode calculated with the effective transport properties obtained from transport measurements (T-LOPC). The dashed red line represents the model for the LOPC mode fitted to the spectra (LOPC) and the dotted red line shows the multi-phonon background (MPB). The solid red line is the sum of the dashed and dotted red lines.

are directly comparable for the two measurement approaches.

As examples, Figure 3A shows the Raman spectra of chips No 15 and 44 in the range between 600 and 1200  $\text{cm}^{-1}$  relative wavenumbers. The Raman spectra are normalised to the peak intensity at 776  $\text{cm}^{-1}$ . The main differences in the spectra occur in the vicinity of the LOPC mode between 950 and 1050  $\text{cm}^{-1}$  as highlighted by the inset. The two spectra demonstrate the sensitivity of the LOPC mode to variations of the charge carrier density and follow the trends described above. The LOPC mode of chip No 44 with the higher  $n_{\text{eff}}$  of  $10^{19} \text{ cm}^{-3}$  at 300 K (determined by the transport experiments) is broadened and shifted to higher wavenumbers in comparison to that of No 15 with the lower  $n_{\text{eff}}$  of  $2 \times 10^{18} \text{ cm}^{-3}$  at 300 K.

Figure 3B,C shows the LOPC part of the Raman spectra of chip No 15 and 44, respectively. The experimental spectra are normalised to the intensity of the LOPC peak. In addition, the two graphs show the calculated line shape (blue solid line) according to Equations (11) to (14) using the transport parameters  $n_{\text{eff}}$  and  $\mu_{\text{eff}}$  determined from the magneto-transport measurements as values for  $n_{\text{eff,R}}$  and  $\mu_{\text{eff,R}}$ , respectively. The SiC material parameters used for the calculations are listed in the supporting information (see Table S2). The quantitative agreement is rather poor. The agreement between experimental data and fitted curve (red dashed line) can already be improved by adjusting  $n_{\text{eff,R}}$  and  $\mu_{\text{eff,R}}$  freely in the LOPC line shape model. A discrepancy at high Raman shifts remains. It arises from the stronger asymmetry of the line shape of the experimentally measured Raman spectrum compared with the LOPC line shape model. A likely origin of this discrepancy is a rather broad and featureless

background due to multi-phonon Raman scattering, which cannot be grabbed by the constant background parameter  $Y$  used in Equation (11). The phonon dispersion relation of 4H-SiC<sup>34</sup> exhibits several modes with phonon energies in wavenumbers of about 500  $\text{cm}^{-1}$  at non-zero wave vectors. We approximate their contribution to the two-phonon Raman scattering processes by a broad Gaussian background centred at about 1000  $\text{cm}^{-1}$ :

$$I_{\text{MP}}(\omega) = k_{\text{MP}} \cdot \exp\left(\frac{-(\omega - \omega_{\text{MP}})^2}{\gamma_{\text{MP}}}\right) \quad (15)$$

where  $k_{\text{MP}}$  is a constant scaling factor,  $\omega_{\text{MP}}$  and  $\gamma_{\text{MP}}$  define the peak position and the line width of the contribution. Adjusting  $n_{\text{eff,R}}$  and  $\mu_{\text{eff,R}}$  freely in the LOPC line shape model and accounting for the multi-phonon background (dotted line) yields in total fitted curves (solid dashed line) which are in almost perfect agreement with the experimental spectra. The parameters for the fit of the Raman spectra are listed in Table S3. The effective charge carrier densities  $n_{\text{eff,R}}$  corresponding to the best fitting curves are  $2.57 \times 10^{18} \text{ cm}^{-3}$  and  $4.32 \times 10^{18} \text{ cm}^{-3}$  for chip No 15 and 44, respectively. The values for  $n_{\text{eff,R}}$  are smaller than the corresponding  $n_{\text{eff}}$  values extracted from the magneto-transport data, but in excellent agreement with the room-temperature free-carrier densities  $n_{300\text{K,CB}}$  of the two specimens extracted with the three-band transport model (see Table S4). This proves that only the free carriers contribute to the carrier plasma, which couples to the optical phonons, and not the localized electrons. However, at room temperature, the localized electrons in the impurity band and the Hubbard state still contribute to the transport as indicated by the

high effective carrier concentrations  $n_{\text{eff}}(300\text{K})$ . These findings are consistent for all samples studied (see Table S4). The findings also underline that a standard analysis of the transport data with a one-band model yielding  $n_{\text{eff}}(T)$  is not sufficient. The value of  $n_{\text{eff}}(T)$  obtained by magneto-transport measurements in case of these highly N-doped 4H-SiC specimens does not simply reflect the free electron concentration, but is a weighted average of the properties assigned to the three parallel transport paths (see Equations (1), and (8)). Furthermore, we find that the effective mobility values  $n_{\text{eff,R}}$ , corresponding to the curves yielding the best fit to the experimental Raman spectrum of the LOPC mode, differ from the conduction band mobilities  $\mu_{\text{CB}}$  of the free electrons determined by fitting the three-band model to the magneto-transport data. The electron mobilities  $\mu_{\text{eff,R}}$  obtained from the Raman data are lower than the conduction band mobilities  $\mu_{\text{CB}}$  from transport data for all four SiC chips studied (see Table S4). The systematic difference between the two mobilities  $\mu_{\text{eff,R}}$  and  $\mu_{\text{CB}}$  is caused by the different experimental conditions and simply reflects the dependence of the mobility on the frequency of the applied electric field. In the magneto-transport measurements, a dc electric field is applied corresponding to 0 Hz. In case of the Raman experiment, the field causing the free carrier plasma coupling to the optical phonons is the light field of the HeNe excitation laser with a wavelength of 633 nm corresponding to a frequency of 474 THz. The dependence of the carrier mobility on frequency derived within the Drude model assumes a frequency-independent relaxation time  $\tau = (m^* \mu_{\text{CB},\omega=0})/e$ . This yields the so called Drude-Smith mobility<sup>35</sup>:

$$\mu_{\text{CB}}(\omega) = \left| \mu_{\text{CB},\omega=0} \frac{1 - \omega^2 \tau^2}{1 - i\omega\tau} \right| \quad (16)$$

where  $\mu_{\text{CB},\omega=0}$  is the electron mobility in the dc case. Its value is determined by the electron mobility of the conduction band electrons in the three-band model extracted from the magneto-transport data.  $m^*$  is the CB effective mass and given in the supporting information (see Table S2). The model yields the right tendency, i.e. that the mobility decreases for external frequencies well above the plasma frequency. However, the qualitative agreement is poor. Using the value for  $\tau$  derived from the magneto-transport experiments, Equation (16) yields a reduction of the mobility at the laser frequency by a factor 1/50. This does not agree well with the experimental finding of a much smaller deviation of about 30% but points in the right direction. This indicates that the assumption of a frequency-independent relaxation time  $\tau$

in the Drude-Smith model does not hold over the required many orders of magnitude in frequency.

So far, we have focused on the comparison of the electrical transport parameters of the N-doped 4H SiC specimens extracted from the magneto-transport and the Raman measurements at room temperature and identified clear trends. We will now turn to a comparison of the temperature-dependent measurements. Exemplarily, Figure 4A shows Raman spectra in the spectral region of the LOPC mode recorded at five different temperatures, which are equally spaced in the range from 100 to 500 K. The Raman signals in the LOPC region reveal a blue-shift with increasing temperature accompanied by a line broadening. It should be noted that, in contrast to the LOPC mode, the LO phonon mode of undoped SiC exhibits a red shift with increasing temperature.<sup>36</sup>

Figure 4B shows the temperature dependence of the effective charge carrier density  $n_{\text{eff,R}}$  resulting from the analysis of all 15 Raman measurements taken between 80 K and 700 K. We accounted for the known red-shift of the intrinsic LO phonon with increasing temperature<sup>36</sup> in the corresponding analysis of the Raman spectrum of the LOPC region. The analysis yields an effective charge carrier density  $n_{\text{eff,R}}$  which, as expected, increases with increasing temperature. This finding is in concordance with the blue-shift of the LOPC peak with increasing temperature. The blue-shift of the LOPC mode occurs despite the red-shift of the intrinsic LO phonon, that of undoped material. Similar effects are known from the literature.<sup>37</sup>

Figure 4B shows a comparison of the temperature dependence of  $n_{\text{eff,R}}$  (open squares) with that of the free carriers  $n_{\text{CB}}$  in the conduction band derived on the basis of the analysis of transport data with the three-band model (solid red line). Significant deviations are observed below 300 K. The values of  $n_{\text{eff,R}}$  are consistently higher between 80 K and 300 K than those extracted from the transport data for the free CB electrons. The dashed red line in Figure 4B shows the magnitude of the deviation and its evolution with temperature. A plausible cause is again the inherently different experimental conditions between the optical and the magneto-transport experiment. In the Raman experiment, the sample volume probed is that in the focus of the excitation laser. The photon energy of the HeNe laser (633 nm) used for excitation is 1.96 eV. It is lower than the SiC band gap, but sufficient to excite electrons from neutral donors  $\text{D}^0$  into the conduction band. Thus, a fraction of the laser light is not scattered, but absorbed yielding additional free electrons in the CB. These photo-excited electrons enhance the density of free carriers, which couple to the optical phonons yielding the LOPC mode. The increase of carrier concentration due to laser excitation has also been



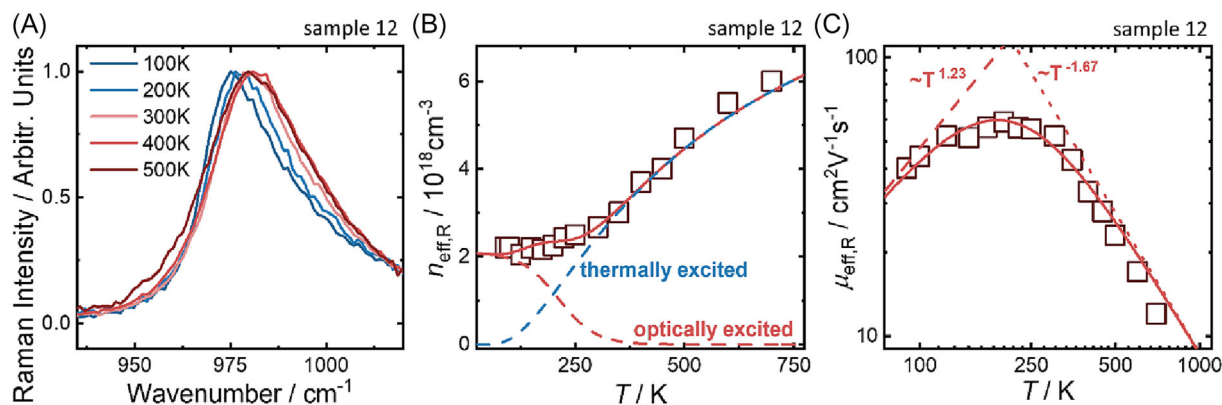


**FIGURE 4** (A) Raman spectra in the vicinity of the LOPC mode of chip no 12 recorded at various temperatures. (B) Temperature-dependent charge carrier density obtained from the Raman measurements (squares). The dashed blue and dashed red lines represent the fractions of electron density thermally and photo-excited into the CB, respectively. The solid red line represents the sum of both excitation mechanisms. (C) Double-logarithmic plot of the temperature dependence of the electron mobility obtained from Raman measurements. The dashed red line represents scattering by impurities and the dotted red line scattering by phonons. The solid red line represents the sum of both scattering mechanisms.

reported for Al-implanted 4H-SiC.<sup>38</sup> Thus, the carrier concentration  $n_{\text{eff,R}}$  measured at the position of the laser spot on the sample is larger than in the transport experiment without illumination. This effect is more pronounced at low temperatures as the fraction of photons absorbed also depends on the number of  $D^0$  states available or in other words the occupation of the impurity band, which decreases with increasing temperature. The deviation approaches zero in the saturation region when all donors are ionized and their electrons are excited to the conduction band. Additional proof was obtained by performing transport measurements with a LED illuminating the sample surface. In this experiment, the sample resistivity was found to decrease with increasing LED intensity.

Figure 4C shows the values of the effective mobility  $\mu_{\text{eff,R}}$  of the electrons extracted from the Raman line shape analysis as a function of temperature. A double logarithmic scale is used. The effective mobility  $\mu_{\text{eff,R}}$  exhibits a maximum at about 250 K. Looking at the slopes of either side of the maximum with values of 1.23 (dashed red line) and  $-1.67$  (dotted red line) at low and high temperatures, respectively, suggests that lattice and impurity scattering dominate the temperature dependence. The values of the slopes in the experiment deviate only slightly from the theoretical values of 1.5 and  $-1.5$  given in the literature for impurity and lattice scattering, respectively.<sup>30</sup> The solid red line represents the sum of both scattering contributions according to Matthiessen's rule, which fits the experimental data mobility quite well. A photograph of the entire N-doped 4H-SiC wafer studied is shown in the supporting information (Figure S1) together with corresponding spatial maps of the free

charge carrier density and the carrier mobility extracted by the Raman analysis based on Equations (11) to (15). A detailed Raman mapping of the free carrier density of chip 24 is depicted in Figure S2. The analysis reveals that colour inhomogeneity and fluctuations of the transport parameters correlate across the wafer.

## 4 | CONCLUSIONS

In highly N-doped 4H SiC samples with doping densities above  $10^{18} \text{ cm}^{-3}$ , but below the insulator-to-metal transition, a careful analysis of the room-temperature Raman spectra of the mode arising from the coupling of the longitudinal phonon with the electron plasma in the conduction band yields the free electron density and their mobility. The carrier density and mobility data obtained by the line shape analysis of the Raman spectra are validated by comparison with magneto-transport data. Due to the high doping, the extraction of the free carrier density of electrons from the magneto-transport data requires fitting the temperature-dependent data in the temperature range from 1.5 K to room temperature by a three-band model. The commonly used one-band model fails and yields too high values. The validation demonstrates that the Raman analysis is indeed a viable approach for assessing and even quantifying doping inhomogeneity of such samples. Thus, multi-channel Raman mapping in conjunction with multivariate data analysis approaches has the potential to be employed as an in-line tool for fast and non-invasive wafer screening in wafer production or the fabrication of semiconductor devices. A thorough investigation of the Raman spectra in the temperature

range between 100 and 700 K reveals the limitations of such an approach, which are inherent to the different experimental conditions in the Raman and the magneto-transport experiment. The values determined for the free electron density by both methods agree well for temperatures above 300 K, however, below 300 K, photoexcitation of electrons from the donor impurity band significantly enhances the free carrier concentration extracted from the Raman spectra. Furthermore, the mobility values obtained from the analysis of the Raman spectra are somewhat lower than those determined by magneto-transport measurements. The reason is the difference in the applied electric field, i.e. a dc field in the case of magneto-transport measurement and an ac field in the THz range in the case of the optical experiment. Nevertheless, the mobility data extracted from temperature-dependent Raman measurements in the range between 100 K and 700 K reveal the expected temperature behaviour with the transition from dominant impurity scattering to dominant phonon scattering.

#### AUTHOR CONTRIBUTIONS

**Hannes Hergert:** Investigation (lead); Validation (equal); Formal analysis (equal); Visualization (equal); Writing—original draft (lead). **Matthias T. Elm:** Formal analysis (equal); Visualization (equal); Supervision (equal); Writing—review & editing (equal). **Peter J. Klar:** Formal analysis (equal); Resources (lead); Visualization (equal); Supervision (equal); Writing—review & editing (equal).

#### ACKNOWLEDGMENTS

We are grateful to the State of Hesse (Hessisches Ministerium für Wissenschaft und Kunst) and the European Union for funding the ERDF-Innovation Laboratory “High Performance Materials”. M.T.E. acknowledges financial support by the Heisenberg Program (grant EL 863/6-1, project number 498993886) from the German Research Foundation (Deutsche Forschungsgemeinschaft). Open Access funding enabled and organized by Projekt DEAL.

#### CONFLICT OF INTEREST STATEMENT

The authors have no conflicts to disclose.

#### ORCID

Hannes Hergert  <https://orcid.org/0000-0001-6257-6185>

Matthias T. Elm  <https://orcid.org/0000-0001-7014-5772>

#### REFERENCES

- [1] S. Doğan, A. Teke, D. Huang, H. Morkoç, C. B. Roberts, J. Parish, B. Ganguly, M. Smith, R. E. Myers, S. E. Saddow, *Appl. Phys. Lett.* **2003**, *82*, 3107.
- [2] H. Bencherif, L. Dehimi, F. Pezzimenti, G. De Martino, F. G. Della Corte, *J. Electron. Mater.* **2019**, *48*, 3871.
- [3] J. W. Palmour, J. A. Edmond, H. S. Kong, C. H. Carter, *Phys. B* **1993**, *185*, 461.
- [4] H. Bartolf, V. Sundaramoorthy, A. Mihaila, M. Berthou, P. Godignon, J. Millan, *Mater. Sci. Forum* **2014**, *778–780*, 795.
- [5] M. Le-Huu, H. Schmitt, S. Noll, M. Grieb, F. F. Schrey, A. J. Bauer, L. Frey, H. Ryssel, *Microelectron. Reliab.* **2011**, *51*, 1346.
- [6] Y. Zhang, D. J. Smith, *J. Semicond.* **2022**, *43*, 041102.
- [7] W. C. Mitchel, W. D. Mitchell, M. E. Zvanut, G. Landis, *Solid-State Electron.* **2004**, *48*, 1693.
- [8] G. Irmer, M. Wenzel, J. Monecke, *Phys. Rev. B* **1997**, *56*, 9524.
- [9] M. T. Elm, P. Uredat, J. Binder, L. Ostheim, M. Schäfer, P. Hille, J. Müßener, J. Schörmann, M. Eickhoff, P. J. Klar, *Nano Lett.* **2015**, *15*, 7822.
- [10] C. H. Will, M. T. Elm, P. J. Klar, B. Landschreiber, E. Güneş, S. Schlecht, *J. Appl. Phys.* **2013**, *114*, 193707.
- [11] R. A. Henning, P. Uredat, C. Simon, A. Bloesser, P. Cop, M. T. Elm, R. Marschall, *J. Phys. Chem. C* **2019**, *123*, 18240.
- [12] K. Yokomoto, K. Shioura, M. Yabu, M. Nakano, N. Ohtani, *Jpn. J. Appl. Phys.* **2020**, *59*, 051003.
- [13] K. Piskorski, M. Guzewicz, M. Wzorek, L. Dobrzański, *AIP Adv.* **2020**, *10*, 55315.
- [14] G. Irmer, W. Siegel, G. Kuhnel, J. Monecke, F. M. M. Yasuoka, B. H. Bairamov, V. V. Toporov, *Semicond. Sci. Technol.* **1991**, *6*, 1072.
- [15] M. Chafai, A. Jaouhari, A. Torres, R. Antón, E. Martín, J. Jiménez, W. C. Mitchel, *J. Appl. Phys.* **2001**, *90*, 5211.
- [16] Z. Mao, C. Fu, X. Pan, X. Chen, H. He, W. Wang, Y. Zeng, Z. Ye, *Phys. Lett. A* **2020**, *384*, 126148.
- [17] T. Takase, M. Sakaino, Y. Sun, T. Miyasato, *Jpn. J. Appl. Phys.* **2013**, *52*, 91301.
- [18] C. Q. Chen, J. Zeman, F. Engelbrecht, C. Peppermüller, R. Helbig, Z. H. Chen, G. Martinez, *J. Appl. Phys.* **2000**, *87*, 3800.
- [19] A. O. Ewvaraye, S. R. Smith, W. C. Mitchel, *J. Appl. Phys.* **1996**, *79*, 7726.
- [20] I. G. Ivanov, A. Henry, E. Janzén, *Phys. Rev. B* **2005**, *71*, 241201.
- [21] W. J. Choyke, in *Proc. of the International Conference on Silicon Carbide, University Park, Pennsylvania, October 20–23, 1968*, (Eds: H. K. Henisch, R. B. T.-S. C. Roy), Elsevier **1969**, S141. <https://doi.org/10.1016/C2013-0-01599-X>
- [22] P. Uredat, P. Hille, J. Schörmann, M. Eickhoff, P. J. Klar, M. T. Elm, *Phys. Rev. B* **2019**, *100*, 85409.
- [23] B. I. Shklovskii, A. L. Efros, *Electronic properties of doped semiconductors*, Springer, Berlin, Heidelberg **1984**.
- [24] H. Iwata, K. M. Itoh, *J. Appl. Phys.* **2001**, *89*, 6228.
- [25] G. Rutsch, R. P. Devaty, W. J. Choyke, D. W. Langer, L. B. Rowland, *J. Appl. Phys.* **1998**, *84*, 2062.
- [26] G. Rutsch, R. P. Devaty, W. J. Choyke, D. W. Langer, L. B. Rowland, E. Niemann, F. Wischmeyer, *Mater. Sci. Forum* **2000**, *338–342*, 733.
- [27] B. K. Meyer, D. Volm, A. Graber, H. C. Alt, T. Detchprohm, A. Amano, I. Akasaki, *Solid State Commun.* **1995**, *95*, 597.
- [28] P. P. Debye, E. M. Conwell, *Phys. Rev.* **1954**, *93*, 693.
- [29] J. Pernot, S. Contreras, J. Camassel, J. L. Robert, W. Zawadzki, E. Neyret, L. Di Cioccio, *Appl. Phys. Lett.* **2000**, *77*, 4359.

- [30] P. Y. Yu, M. Cardona, *Fundamentals of semiconductors*, Third, Rev. ed., Springer, Berlin, Heidelberg **2005**.
- [31] G. Irmer, V. V. Toporov, B. H. Bairamov, J. Monecke, *Phys. Status Solidi A* **1983**, 119, 595.
- [32] M. V. Klein, B. N. Ganguly, P. J. Colwell, *Phys. Rev. B* **1972**, 6, 2380.
- [33] W. L. Faust, C. H. Henry, *Phys. Rev. Lett.* **1966**, 17, 1265.
- [34] M. Hofmann, A. Zywiets, K. Karch, F. Bechstedt, *Phys. Rev. B* **1994**, 50, 13401.
- [35] R. Ulbricht, E. Hendry, J. Shan, T. F. Heinz, M. Bonn, *Rev. Mod. Phys.* **2011**, 83, 543.
- [36] M. Bauer, A. M. Gigler, A. J. Huber, R. Hillenbrand, R. W. Stark, *J. Raman Spectrosc.* **1867**, 2009, 40.
- [37] H. Y. Sun, S.-C. Lien, Z. R. Qiu, H. C. Wang, T. Mei, C. W. Liu, Z. C. Feng, *Opt. Express* **2013**, 21, 26475.
- [38] T. Liu, Z. Xu, M. Rommel, H. Wang, Y. Song, Y. Wang, F. Fang, *Crystals* **2019**, 9, 9.

### SUPPORTING INFORMATION

Additional supporting information can be found online in the Supporting Information section at the end of this article.

**How to cite this article:** H. Hergert, M. T. Elm, P. J. Klar, *J Raman Spectrosc* **2023**, 54(7), 737.  
<https://doi.org/10.1002/jrs.6531>